Plasmonic Coupling of Au Nanoclusters on a Flexible MXene/Graphene Oxide Fiber for Ultra-sensitive SERS Sensing

Journal:	*ACS Sensors*
Manuscript ID	se-2022-02808c.R1
Manuscript Type:	Article
Date Submitted by the Author:	04-Feb-2023
Complete List of Authors:	LIU, XIN; NPU, School of materials science and engineering Dang, Alei; Northwestern Polytechnical University, Materials Sicence & Engineering Li, Tiehu; Northwestern Polytechnical University, Sun, Yiting; Northwestern Polytechnical University, Lee, Tung-Chun; University College London, Institute for Materials Discovery Deng, Weibin; Northwestern Polytechnical University Wu, Shaoheng; Northwestern Polytechnical University Zada, Amir; Abdul Wali Khan University Mardan Zhao, Tingkai; Northwestern Polytechnical University, School of Materials Science and Engineeering Li, Hao; Northwestern Polytechnical University,

Plasmonic Coupling of Au Nanoclusters on a Flexible MXene/Graphene Oxide Fiber for Ultra-sensitive SERS Sensing

Xin Liu[1,2], Alei Dang[1,2*], Tiehu Li[1,2*], Yiting Sun [1,2], Tung-Chun Lee[3,4], Weibin Deng[1,2], Shaoheng Wu[1,2], Amir Zada[5], Tingkai Zhao[1,2], Hao Li[1,2]

[1.] School of Materials Science and Engineering, Northwestern Polytechnical University, Xi'an 710072, P. R China

[2.] Shannxi Engineering laboratory for Graphene New Carbon Materials and Applications, School of Materials Science and Engineering, Northwestern Polytechnical University, Xi'an 710072, P. R China.

[3.] Department of Chemistry, University College London (UCL), London WC1H 0AJ, U.K

[4.] Institute for Materials Discovery, University College London (UCL), London WC1H 0AJ, U.K

[5.] Department of Chemistry, Abdul Wali Khan University Mardan, 23200, Pakistan.

***Corresponding author：Alei Dang, Tiehu Li,**

E-mail address: dangalei@nwpu.edu.cn; litiehu@nwpu.edu.cn

Abstract: High sensitivity, good signal repeatability, and facile fabrication of flexible surface enhanced Raman scattering (SERS) substrates are common pursuits of researchers for the detection of probe molecules in the complex environment. However, fragile adhesion between the noble nanoparticles and substrate material, low selectivity and complex fabrication process on a large-scale limit SERS technology for the wide-ranging applications. Herein, we propose a scalable and cost-effective strategy to fabricate sensitive and mechanically stable flexible $Ti_3C_2T_x$ MXene@graphene oxide/Au nanoclusters (MG/AuNCs) fiber SERS substrate from the wet spinning and subsequent in-situ reduction processes. The employ of MG fiber provides good flexibility (114 MPa) and charge transfer enhancement (chemical mechanism-CM) for SERS sensor and allows further in-situ growth of AuNCs on its surface to build highly sensitive hotspots (electromagnetic mechanism-EM), promoting the durability and SERS performance of substrate under complex environments. Therefore, the formed flexible MG/AuNCs-1 fiber exhibits a lowest detection limit at 1×10^{-11} M with a 2.01×10^{9} enhancement factor (EF_{exp}), signal repeatability (RSD=9.80%) and time retention (remains 75% after 90 days storage) for R6G molecules. Furthermore, the L-cysteine modified MG/AuNCs-1 fiber realized the trace and selective detection of trinitrotoluene (TNT) molecules (0.1 μM) via Meisenheimer complex formation, even by sampling the TNT molecules at fingerprint or sample bag. These findings fill the gap in the large-scale fabrication of high-performance 2D materials/precious metal particle composite SERS substrates, and expect to push flexible SERS sensors towards wider applications.

Keywords: SERS, MXene, Au nanocluster, wet-spinning, flexible fiber, 2D materials

In recent decades, the sustainable and scalable fabrication of surface-enhanced Raman scattering (SERS) substrates with high sensitivity and stability has been critical for the detection and imaging of analytes for applications in food safety, national defense, environmental monitoring, biological and biomedical fields, and many more[1-4]. To achieve a high-performance SERS substrate, a variety of novel materials ranging from noble metals (such as Au, Ag and Cu)[1-3, 5-8], crystal/amorphous semiconductors[9-12], metal-organic frameworks[13] to two-dimensional (2D) materials (e.g. graphene[14], boron nitride[15], metal carbides and/or nitrides-MXene[16-18], and transition metal chalcogenides-TMDs[19]) have been successively explored since their discovery in 1974 by Fleischmann et. al[20]. Among these materials, plasmonic structures assembled from Au or Ag nanoparticles have been substantially studied due to their ability to generate localized surface plasmon resonance (LSPR) excited by the incident light on the plasmonic nanostructure, which is bestowing on the electromagnetic mechanism (EM) for SERS enhancement[1, 2]. However, spontaneous aggregation and random dispersion of noble metal nanoparticles leads to more than 50% signal fluctuation during detection at different times, which is almost impossible to use for quantitative analysis[1, 21]. To address these challenges, emerging strategies have been shifted from monodisperse noble metal nanoparticles to the construction of large-area and highly SERS-active nanoparticles via chemical modification or lithography techniques on the surface of rigid (e.g., silicon, quartz, glass) [22, 23]or flexible materials[24, 25] in a controlled way.

Compared to rigid materials, flexible materials are widely favored among researchers due to their advantages of low cost, multi-functionality and especially

"flexibility" in practical applications[26, 27]. For instance, in the application of probe molecules monitoring, SERS detection for rigid substrates requires tedious sample collection and extraction before the analysis process, while flexible substrates can collect analytes directly from suspected target surfaces through easy-to-operate steps, such as "wiping" or "sticking"[28]. Generally, two types of flexible materials have been extensively investigated as substrates for noble metal nanoparticles: active material substrates (e.g., graphene[14] and carbon nanotubes[29]), mainly derived from charge transfer (CT) between the substrate and probe molecules, which is defined as the chemical mechanism (CM), and non-active material substrates (e.g., filter paper[30], elastomers[31, 32], plastics[5, 24]) without CM and EM contributions to SERS enhancement. For the former, the produced plasmonic structure tends to be lost during sampling due to the low adhesion between precious metals and substrate materials, which substantially deteriorates the stability and reproducibility. For the latter, the sensitivity for the detection of probe molecules could be greatly influenced due to the absence of the dedication of either CT or plasmonic coupling from the substrate.

Two-dimensional transition metal carbides, nitrides or carbonitrides (MXenes), as a rapidly expanding family of 2D materials, have attracted attention owing to their good hydrophilicity and biocompatibility, high metallic conductivity, adjustable electronic structure, cost-effective fabrication and outstanding flexibility[16, 17, 33]. Due to the above-mentioned metrics, they have not only been exploited in flexible electronics[34] and photonics devices[35], but can also be directly used as a SERS substrate or flexible materials to complement CM in addition to the EM effect of noble metal

nanoparticles[36-38]. For instance, Yu et al. reported a $Ti_3C_2T_x$/Au nanorod (AuNR) composite prepared by the electrostatic adsorption of $Ti_3C_2T_x$ and AuNRs[36]. It demonstrated the detection limits of 10^{-12}, 10^{-12} and 10^{-10} M for R6G, crystal violet (CV) and malachite green (MG) molecules, respectively, despite a silicon rigid substrate used during the monitoring process. Furthermore, due to the unsaturated oxidation state of its terminal metal atoms, MXene could also be used directly as a reductant to reduce metal cations to metallic nanoparticles via the spontaneous donation of electrons from MXene[39, 40] to produce the more strongly binding MXene@noble nanoparticle hybrid SERS substrate [37, 38]. Despite the great potential, current research has focused on hybrid colloidal solutions or small pieces of film substrate levels and has rarely reported the fabrication of these substrates with large-scales and macro sizes, but it is critical for bringing SERS technology out of the lab. Moreover, the enhancement mechanism, time retention and stability, and mechanical performance of the formed flexible MXene/noble nanoparticle SERS substrates have rarely investigated systematically, particularly for the monitoring of explosive residue molecules.

At present, more than 20 MXenes have been experimentally synthesized, and many new MXenes are being theoretically predicted and continually exploited based on the more than 70 MAX ceramic phases[33, 41], endowing their potential usage in SERS substrates from the laboratory to real world. Considering that graphene oxide liquid crystals (LCs) can promote the spin-ability of $Ti_3C_2T_x$ MXene owing to their paramount liquid crystalline features in solution[42], herein, a scalable, facile and cost-effective strategy is proposed to fabricate a sensitive and stable flexible fiber substrate on a large

scale for practical SERS substrates. By virtue of the liquid crystal (LC) self-assembly of $Ti_3C_2T_x$ MXene and graphene oxide (GO) colloidal hybrids and the reduction property of $Ti_3C_2T_x$ nanosheets, flexible MG/Au nanoclusters (AuNCs) fibers over 10 meters long scale can be prepared within a couple of minutes. Benefiting from the plasmon coupling from the dense AuNCs and the photo-induced charge transfer (PICT) process of $Ti_3C_2T_x$ MXene, the Raman signal was significantly enhanced by the combination of EM and CM effects. Furthermore, flexible fibers also demonstrated a good signal repeatability, strong oxidation resistance and excellent mechanical stability, thus promising their rapid and reliable on-site SERS detection. Owing to these impressive features, the explosive residues (trinitrotoluene-TNT and trinitroaniline-Tetryl) with ultra-low concentration were selectively identified by using L-cysteine modified flexible MG/AuNCs-1 fiber sensor on fingerprint and sample bag. This work has therefore significant implications for understanding the SERS mechanism of MXene/noble metal flexible substrates and supporting SERS technology towards practical applications.

Experimental Part

Materials

Ti_3AlC_2 powder was purchased from Laizhou Kaiene Ceramic Material Co., Ltd (Shandong, China). Chloroauric acid ($HAuCl_4 \cdot 4H_2O$, ≥99.99%), hydrochloric acid (HCl, 36-38%), graphite powder (C, ≥99.85%), potassium permanganate ($KMnO_4$, ≥99.5%), sulfuric acid (H_2SO_4, 95~98%), phosphoric acid (H_3PO_4, ≥85.0%), absolute ethanol, potassium persulfate ($K_2S_2O_8$, ≥99.5%), hydrogen peroxide (H_2O_2, ≥30.0%), anhydrous calcium chloride ($CaCl_2$, ≥96.0%), 2,4-dinitrotoluene (DNT) ($C_7H_6N_2O_4$, ≥99.99%), 4-nitrophenol (4-NTP) ($C_6H_5NO_3$, ≥99.99%), nitrobenzene (NB) ($C_6H_5NO_2$, ≥99.99%) and L-cysteine ($C_3H_7NO_2S$, ≥97.0%) were purchased from Sinopharm Chemical Reagent Co., Ltd (Shanghai, China). Lithium fluoride (LiF, ≥99.0%) was obtained from Macklin. Rhodamine 6G ($C_{28}H_{31}N_2O_3Cl$, ≥99.0%) was purchased from Aladdin. 2,4,6-trinitrotoluene (TNT, $C_7H_5N_3O_6$, ≥ 99.9%) and 2,4,6-trinitroaniline (Tetryl) ($C_7H_5N_5O_8$, ≥99.9%) were purchased from the National Standards Center (Zhengzhou, China). Deionized water (DI, homemade) was used throughout the experiments. All chemicals were used directly without purification.

Synthesis of $Ti_3C_2T_x$ MXene@AuNCs hybrids

To explore the growth mechanism of AuNCs on $Ti_3C_2T_x$ MXene nanosheets, 1 mL $HAuCl_4$ aqueous solution with different concentrations (0.1, 0.5, 1, 5 and 10 mM) was separately added to a colloidal suspension of 1 mL 0.1 mg/mL $Ti_3C_2T_x$ MXene and sonicated at a speed of 100 rpm at room temperature. After 2 min growth, the formed

hybrid colloidal suspensions of different colors were obtained. Finally, the colloidal suspensions were centrifuged at 6000 rpm for 5 min to remove excess reactants, and re-dispersed in DI water for further characterization. Herein, the preparation process of $Ti_3C_2T_x$ nanosheets and the growth mechanism of AuNCs on $Ti_3C_2T_x$ MXene nanosheets and MG fiber can be found in detail at the Supplementary Materials.

Flexible MG/AuNCs fiber SERS substrates

First, a series of $Ti_3C_2T_x$ MXene/GO (noted as MG) fibers with different GO contents (5, 10, 20, 30, 40 and 50 wt%) were prepared by wet spinning method (see details in **Supplementary Materials**). Due to the full coverage of $Ti_3C_2T_x$ MXene on the surface of MG-20 fiber (see details in the **Discussion**) to provide suitable active sites for the reduction of metal cations, the MG-20 fiber was thus employed for the fabrication of following MG/AuNCs fiber SERS substrates. Typically, MG-20 was cut into 10 cm, and immersed in 5 mL solution of 1 mM $HAuCl_4$ for the in-situ reduction of Au(III) to zero-valent Au under continuous stirring for 2 min. The MG/AuNCs fiber substrate was then obtained after rinsing three times by DI water and dried at 60 ^{o}C for 24 h. The functional fiber substrate was denoted as MG/AuNCs-0.1 where 0.1 mM denotes the concentration of $HAuCl_4$ solution. Other samples containing 0.5, 1, 5 and 10 mM $HAuCl_4$ solution were also prepared following the same procedure and denoted as MG/AuNCs-0.5, MG/AuNCs-1, MG/AuNCs-5 and MG/AuNCs-10, respectively.

Characterization

Atomic force microscopy (AFM, Dimension Icon, Bruker) was employed to

measure the lateral dimensions and thickness of GO and $Ti_3C_2T_x$ MXene nanosheets. The morphologies and EDS spectra of the $Ti_3C_2T_x$ MXene@AuNCs hybrid sheets and all fiber substrates were recorded using scanning electron microscopy (SEM, Verios G4, 5 kV) and transmission electron microscopy (TEM, Talos F200X, 200 kV) equipped with an energy dispersive spectroscopy system (NORAN System 7) respectively. The phase structure of the samples was analyzed by a power X-Pert PRO X-ray diffractometer (XRD) (Cu Kα1, λ = 0.154 nm). X-ray photoelectron spectroscopy (XPS, Thermo Scientific TM K-Alpha TM$^+$ spectrometer, Al Kα X-ray source, *hv*=1486.6 eV) was employed to characterize the chemical compositions of the samples. All peaks were calibrated with the C1s peak binding energy at 284.8 eV for adventitious carbon. To clarify the light absorption of the samples, ultraviolet-visible (UV–Vis) absorption spectra were obtained with a TU-1810PC UV–vis spectrometer (Persee, Beijing). The mechanical properties of all the fibers were cut into the length of 8 cm and further measured by an intelligent electronic tensile testing machine (INSTRON, HP-5). In SERS tests, all spectra of the samples were obtained using an Alpha300R confocal Raman microscope (WI Tec) with an excitation wavelength of 532 nm. Unless specifically noted, the laser power was 0.1 mW, the specification of the objective was ×50 L, and the acquisition time was kept at 5 s. Moreover, for the detail detection process of R6G and nitroexplosive molecules on MG/AuNCs SERS substrate, corresponding calculation of the enhancement factor (EF) and the simulation of the theoretical electromagnetic field intensity on the fiber substrate were demonstrated in the Supporting Information.

Results and Discussion

The strategy of wet-spinning assembly is known as a green and facile method to assemble two-dimensional (2D) colloidal nanosheets, such as graphene and MXene nanosheets on the fibers on a large scale[43, 44]. Nevertheless, the MXene nanosheets with a small lateral size (200-700 nm, **Figure S1**) are difficult to assemble on the fiber with high flexibility and a meter-scale length due to the weak interlaminar force between the nanosheets. With that in mind, graphene oxide liquid crystal (LC) with a large lateral size of 5~30 μm (**Figure S2**) was employed as a template to promote the spin-ability of $Ti_3C_2T_x$ MXene owing to its outstanding liquid crystalline features in solution. **Figure 1a** schematically demonstrates the fabrication process of the flexible fiber SERS substrate with high flexibility. Owing to the coulombic force between the negative $Ti_3C_2T_x$ MXene and GO layers via Ca^{2+} ions in the $CaCl_2$ coagulation bath, a meter-long $Ti_3C_2T_x$ MXene/GO fiber (noted as MG fiber) was obtained and collected on the spool (**Figure 1b**). Moreover, with different contents (5, 10, 20, 30, 40 and 50 wt%) of GO, the tensile strength of the as-synthesized MG fibers gradually augmented from 73.6 MPa to 174.3 MPa due to the improved van der Waals forces and uniform orientation of $Ti_3C_2T_x$ and GO sheets along the axis of fibers. This indicates that the MG fibers have sufficient mechanical strength to provide their potential for SERS sensing in complex environments (**Figure S3**). **Figure 1c** shows the SEM image and the corresponding energy disperse spectroscopy (EDS) mapping of C and Ti elements in the MG fiber. Evidently, the orientation of $Ti_3C_2T_x$ MXene nanosheets along the axial direction of the fibers and the well-distributed Ti elements can be observed which

demonstrates the successful fabrication of MG fibers.

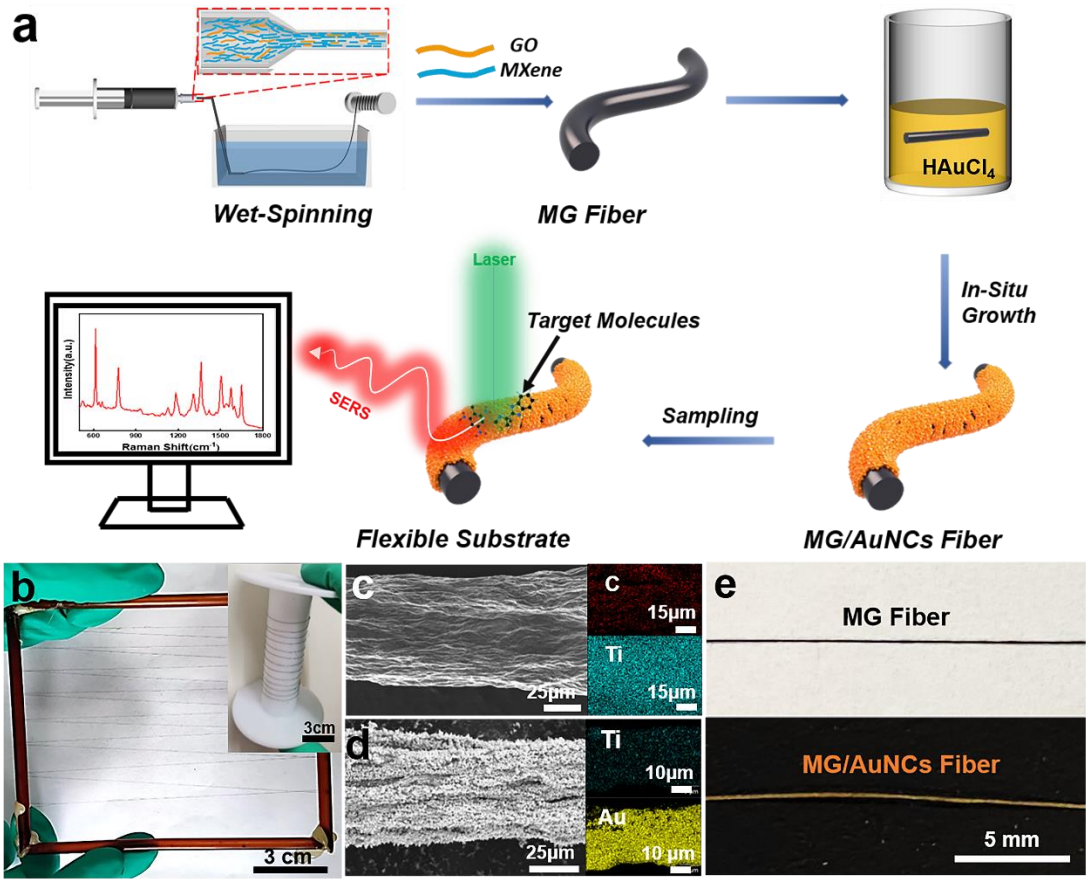

Figure 1. (a) Schematic illustration of the large-scale preparation process of flexible MG/AuNCs fiber substrates and SERS detection of target molecules. (b) Digital image of as-produced MG/AuNCs-1 fiber with meter-scale. Insert in (b): The MG/AuNCs-1 fiber was collected on the roller. SEM images of MG (c) and (d) MG/AuNCs-1 fiber and the corresponding C, Ti and Au EDS mapping. (e) The digital photographs of MG and MG/AuNCs-1 fibers.

From theoretical study, $Ti_3C_2T_x$ MXene nanosheets enabled the spontaneous donation of electrons to reduce noble metal cations (Au, Ag and Pd) into their corresponding metal nanoparticles due to the unsaturated oxidation state of their terminal Ti atoms[37-40]. Thus, the fabricated MG fiber has good potential as a reductant

for the direct reduction of metal cations. **Figure 1d** demonstrates the SEM image of the formed MG/AuNCs-1 fiber, indicating that the functional composite fiber can be facilely fabricated when the MG fiber is immersed in 1 mM chloroauric acid ($HAlCl_4$) aqueous solution for 2 min at room temperature (**Figure 1a**) even in the absence of surfactant in the growth solution. The elemental mapping of EDS further proves the uniform element distribution of Au on the surface of the MG fiber (**Figure 1c and d**), which can subsequently serve as an ideal SERS substrate with high sensitivity and signal consistency. Moreover, the MG/AuNCs fiber was golden yellow in color, while the pristine MG fiber was black (**Figure 1e**). These changes in the visual appearance further indicated the success of the in-situ growth of AuNCs.

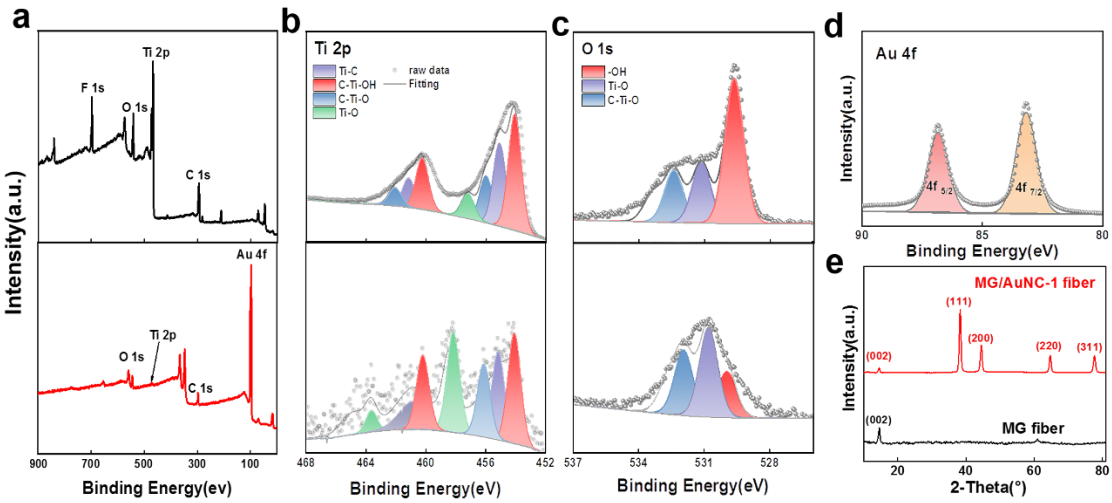

Figure 2. Comparison of XPS spectra of MG and MG/AuNCs-1 fibers: (a) wide survey spectrum; core level spectra of the (b) Ti 2p, (c) O 1s and (d) Au 4f regions. (e) XRD spectra of MG and MG/AuNCs-1 fiber.

To interpret the reducing mechanism of the MG fiber, X-ray photoelectron spectroscopy (XPS) and X-ray diffraction (XRD) studies of MG and MG/AuNCs-1

fiber substrates were carried out. From the XPS spectra (**Figure 2a)**, Ti, C and O can be observed in the MG fiber before and after the reduction of $HAuCl_4$. Compared to the MG fiber, the newly appeared peak at 83.17 eV is mainly attributed by AuNCs (**Table S2**) at MG/AuNCs-1 fiber while the disappeared peak at 684.08 eV belongs to F, which is mainly led by the full coverage of AuNCs on the MG fiber. Moreover, the original high-resolution Ti 2p spectra can be deconvoluted into four main components: Ti-C, C-Ti-OH, C-Ti-O and Ti-O bonds (**Figure 2b**). After reduction, the fraction of C-Ti-O and Ti-O bonds in the MG/AuNCs-1 fiber increases substantially, while the C-Ti-OH decreases rapidly. According to the previous studies[38], the -OH functional group-terminated Ti atoms in $Ti_3C_2T_x$ MXene are more unsaturated, and thus, they have a higher reducing power than Ti atoms terminated by –O groups. Consequently, the Ti atoms terminated by the -OH group in the MG fiber can donate electrons to Au(III), and the corresponding C-Ti-OH bands are oxidized to C-Ti-O or Ti-O, resulting in increased Ti-O bond area from 9.6% to 27.3%. Correspondingly, the 529.65 eV peak corresponded -OH groups is almost disappeared after the reduction of Au(III) to metallic Au in the high-resolution XPS spectra of O1s (**Figure 2c**). This indicates the higher reducibility of MG fibers as their counterpart $Ti_3C_2T_x$ MXene. Moreover, two-extra peaks at 83.17 eV and 86.82 eV rooted from Au can be probed on the MG/AuNCs-1 fiber substrate (**Figure 2d**), verifying the formation of AuNCs. Finally, the crystalline structure of the fibers was investigated by XRD (**Figure 2e).** From the patterns, compared with the MG fiber, four additional diffraction peaks appeared on

MG/AuNCs-1, which corresponded to the (311), (220), (200) and (111) crystalline planes of metallic Au with a face-centered cubic structure.

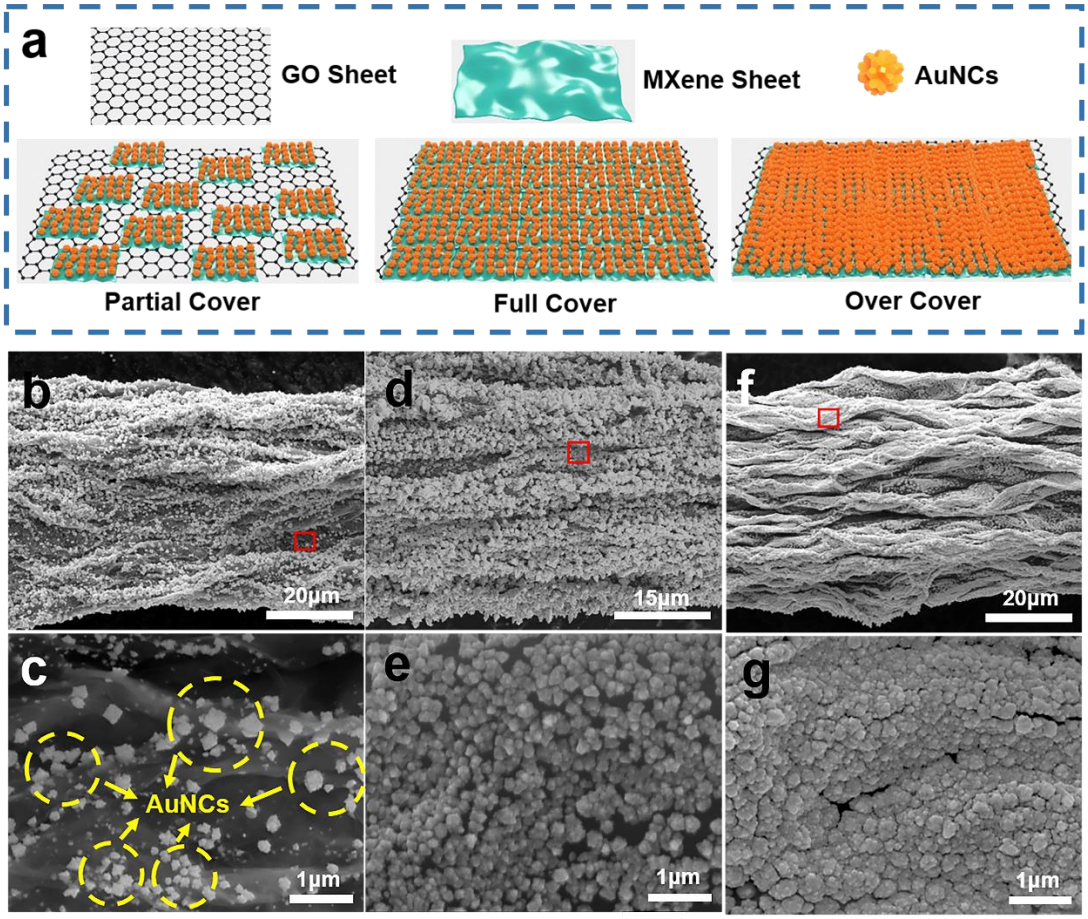

Figure 3. (a) Schematic illustration of GO-mediated AuNCs growth on MG fibers. (b-g) Representative SEM images of as-synthesized MG/AuNCs fibers with different contents of GO in the range of (b) 50 wt%, (d) 20 wt% and (f) 5 wt% respectively, and their corresponding enlarged areas (c, e and g) outlined by the red rectangle in (b, e and d). The formed AuNCs nanostructures with sparse distribution are highlighted by dashed line with yellow color in (c).

The content of GO in the spinning solution is an important parameter to adjust the distribution of $Ti_3C_2T_x$ MXene nanosheets (active sites) on the surface of the MG fibers,

which determines the assembled structures and their corresponding plasmon coupling. To optimize the uniformity of Raman signal and achieve the maximum plasmon coupling, MG/AuNCs fiber substrates with different contents of GO (5, 10, 20, 30, 40 and 50 wt%) were fabricated via immersing the corresponding MG fiber in 1 mM $HAuCl_4$ growth solution. **Figure 3a** shows a schematic illustration of the GO-mediated AuNCs distribution on MG fibers, where the formed nanostructures are substantially influenced by the variation of $Ti_3C_2T_x$ nanosheets's content.

Figure 3b-g and Figure **S4a-f** show the SEM images of produced MG/AuNCs fibers. As the contents of GO decreases from 50 to 30 wt%, the number densities of AuNCs are obviously augmented owing to the increase of $Ti_3C_2T_x$ MXene on the surface of the fibers (**Figure 3b, c** and **Figure S4a-d)**, which provides more active sites for the reduction of Au(III) to metallic Au. However, due to the limited $Ti_3C_2T_x$ MXene nanosheets, the assembled structure formed (circled by the yellow dashed line) could only be partially covered by the reduced AuNCs. As the contents of GO decreases to 20 wt%, it is obvious that the formed AuNCs are densely populated on the surface of fiber with a small interparticle distance (**Figure 3d, e**). This greatly contributes to the substantial increase in the number density and uniformity of plasmonic hot-spots, as schematically illustrated in **Figure 3a**. Nevertheless, when the content of GO further decreased to 10 and 5 wt%, the AuNCs are merged together due to the more redox sites provided by the superimposed $Ti_3C_2T_x$ for the reduction of Au (III) (**Figure S4e, f and Figure 3f, g**), and lead to the loss of hot-spots.

To assess the potential of the flexible MG/AuNCs fibers as SERS substrates, we

measured the detection limit of R6G molecules on the optimized MG/AuNCs-1 fiber. **Figure 4a** shows all SERS spectra of R6G molecules with concentrations from 1×10^{-4} M to 1×10^{-11} M collected from the MG/AuNCs-1 fiber surface under 532 nm excitation. The characteristic peaks at 612, 774 and 1650 cm^{-1} can be distinctly detected even when the concentration of R6G molecules is decreased to 1×10^{-11} M (**Figure S5**), indicating that MG/AuNCs-1 substrate has a higher sensitivity than previously reported (Table 1). This can be ascribed to the synergistic effect of the strong plasmon coupling between the AuNCs, the combination of AuNCs and $Ti_3C_2T_x$ MXene sheets in MG fibers (EM and CM) and the charge transfer (CT) of electrons from probe molecules to AuNCs. Thus, a high EF_{exp} is obtained at 2.01×10^{9}. Moreover, there is a good linear relationship for the plot of SERS intensities of the peak at 612 cm^{-1} versus the concentration of R6G with a correlation coefficient (R^2) of 0.956 (**Figure 4b**), which shows that the MG/AuNCs substrate is a potential candidate for the quantitative and quick detection of dye molecules at ultralow concentration.

Table 1. Detection sensitivity of SERS substrates in previously reported and this work

Materials	Molecules	Sensitivity	with flexibility	Ref.
$Ti_3C_2T_x$ MXene	R6G	10^{-7} M	No	16
$Ti_3C_2T_x$ -AgNPs	4-MBA	10^{-8} M	No	45
Nb_2C	MeB	10^{-8} M	No	46
Ta_2C	MV	10^{-7} M	No	46
$Ti_3C_2T_x$ -AuNRs	MG	10^{-10} M	No	36
$Ti_3C_2T_x$ /MoS_2-AuNPs	Cy5	10^{-9} M	No	47
$Ti_3C_2T_x$ -AuNCs	R6G	10^{-11} M	Yes	This Work

For practical applications, the signal reproducibility, uniformity and stability are key parameters for the reliable flexible SERS substrates. The SERS intensities of R6G (1×10^{-4} M) were recorded at 200 random points across the entire MG/AuNCs-1 fiber to evaluate the reproducibility in space, as shown in **Figure 4c**. This illustrates that the Raman signals are relatively consistent at arbitrary points. The relative standard deviation (RSD) value of R6G in the intensity at the characteristic peak (612 cm^{-1}) is less than 9.56% (**Figure 4d**), indicating the paramount homogeneity and reproducibility of MG/AuNCs-1 fiber, which is much lower than many other previously reports[36, 38], especially for colloidal substrates. These results were further supported by Raman mapping on the fiber surface (**Figure S6**). The excellent SERS signal repeatability of the MG/AuNCs-1 fiber is mainly from the macroscopic uniformity, as shown in **Figure 4e**.

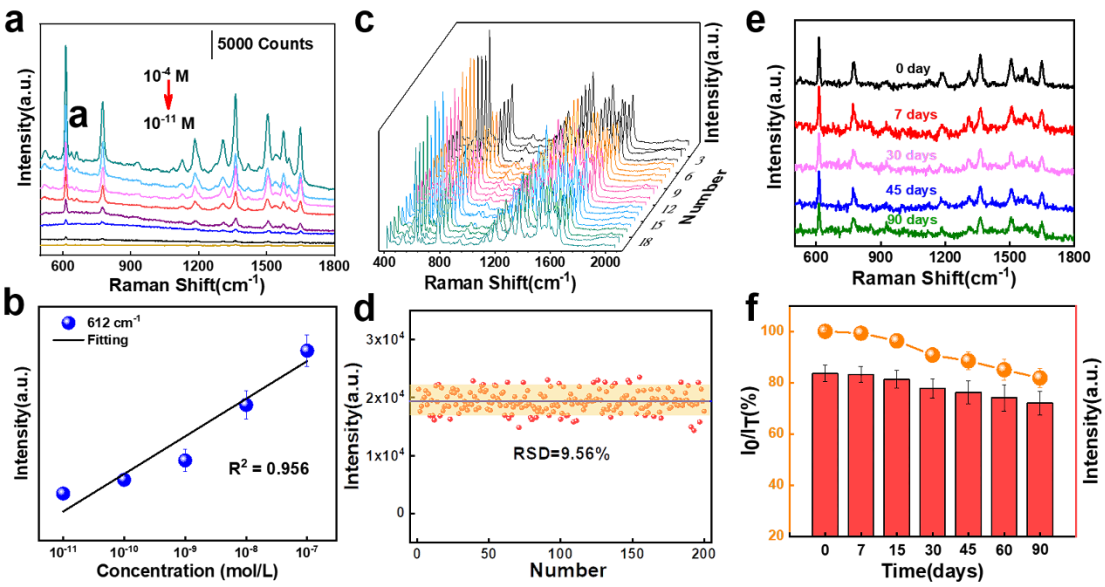

Figure 4. (a) SERS intensities of R6G molecules from 1×10^{-4} to 1×10^{-11} M on the MG/AuNCs-1 fiber substrate. (b) Corresponding Raman intensities of R6G molecules at 612 cm^{-1} with different

concentrations. (c) SERS intensities of 10^{-4} M R6G recorded from 20 randomly selected positions from the MG/AuNCs-1 fiber substrate and (d) the corresponding intensity at 612 cm^{-1} band (the average value is plotted with the gray line, and the yellow region illustrates the variation in intensity at ±9.56). (e) The attenuation of SERS spectra of R6G at 612 cm^{-1} on the surface of MG/AuNCs-1 fiber substrate stored in the ambient environment at various times from 0 to 90 days and (f) corresponding Raman intensity change versus times at 612 cm^{-1}.

The weak oxidation resistance of MXene nanosheets gives a strict limitation for practical applications[33]. Therefore, the time repeatability of the SERS substrate was estimated by monitoring the Raman intensity of target molecules with different storage times. As plotted in **Figure 4e,** the Raman intensities of R6G molecules (10^{-8} M) remain consistent in the first 30 days compared with the initial samples (0 days). After 90 days of storage, the Raman signal at 612 cm^{-1} still retains 75% signal intensity (**Figure 4f**). This can be attributed to the successful coverage of stable AuNCs, which prevent the oxidation of $Ti_3C_2T_x$ MXene on the outside layers of MG fiber, making the fiber substrate more stable and enabling longer storage time. To investigate this effect, the XRD patterns of the MG/AuNCs-1 and pristine MG fibers at different exposure times to air were demonstrated in **Figure S7.** For the MG fibers, after 30 days of exposure to air, a new peak at 25.25° appeared, which is mainly derived from the oxidation of Ti atoms on the $Ti_3C_2T_x$ MXene to TiO (101), while it is not observed in the MG/AuNCs-1 fiber even stored for 90 days. This result verifies that the in situ reduced AuNCs not only provide superior sensitivity and signal homogeneity, but also possess with the advantages of repeatability in time and space by limiting air contact to postpone the

oxidation process of the MG fiber substrate.

In addition to the SERS performance, the mechanical stability of the flexible SERS substrate is another crucial parameter for practical application. As shown in **Figure 5**, the mechanical stimuli such as bends and twists were used to characterize the mechanical stability of the resultant MG/AuNCs-1 fiber substrate. After bending the MG/AuNCs-1 fiber with an angle of 75° and twisting to 135° respectively for 500 cycles (Inset in **Figure 5a, c**), the AuNCs were still attached to the surface of the MG fiber, although the distances between the individual AuNCs slightly vary under different mechanical stimuli (**Figure S8**).

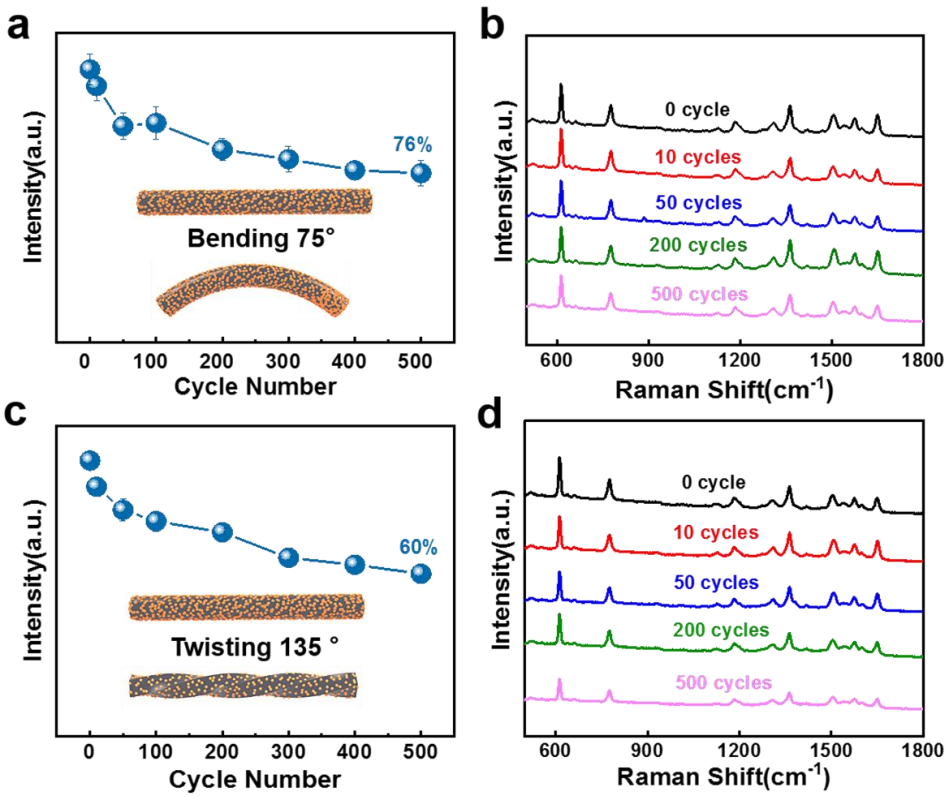

Figure 5. The SERS intensities of MG/AuNCs-1 fiber substrate varies with the different mechanical stimuli. (a) and (c) The attenuation of the Raman signal of R6G (1×10^{-4} M) at 612 cm^{-1} on the MG/AuNCs-1 fiber in the length of 8 cm for 500 bending and twisting cycles. Inset in (a) and (c):

the schematic of bending and twisting of MG/AuNCs-1 fiber. (b) and (d) the corresponding Raman spectra of molecules at different cycles.

The Raman intensities of R6G molecules (10^{-4} M) on the fiber substrate were obtained after each mechanical deformation. After bending and twisting for 500 cycles, the MG/AuNCs-1 fiber still remains 76% and 60% Raman signal intensities of the band at 612 cm^{-1} respectively (**Figure 5a, c**), in contrast to its initial state without mechanical deformation. They are mainly derived from the strong chemical bonds between the MG fiber and reduced AuNCs, and the extraordinary flexibility of the MG fiber substrate material (114 MPa, **Figure S3**), displaying good mechanical durability and the retention of Raman intensity (**Figure 5b, d**). Those merits endow its potential application in actual monitoring of analytes on nonplanar surfaces for direct sampling. Meanwhile, the decrease in Raman signal after mechanical stimuli is probably caused by slight sliding of each $T_3C_2T_x$ MXene nanosheets within the fibers, leading to changes in the assembled structure from AuNCs attachment to the MXene sheets. Thus, a few cracks can be observed on the surface of the MG fibers after 500 cycles of twisting (**Figure S8**).

Figure 6a illustrates the schematic diagram of SERS detection of analytes (R6G) that are adsorbed on the surface of AuNCs or located in the gap between AuNCs. As reported previously, the SERS performance is substantially influenced by the gap size between adjacent AuNCs due to the gap-dependent plasmon coupling effect. To understand the underlying mechanism of Raman signal enhancement on the as-synthesized MG/AuNCs-1 fiber substrate, finite element method (FEM) was employed

to assess electric field enhancement effects. Specifically, the EF from the simulation (denoted as EF_{sim}) is proportional to $|E_{max}/E_0|$, as demonstrated in formula (1):

$$EF_{sim} = \left|\frac{E_{max}}{E_0}\right|^4 \quad (1)$$

where the E_{max} and E_0 are the intensities of the maximum electromagnetic field and the incident field, respectively.

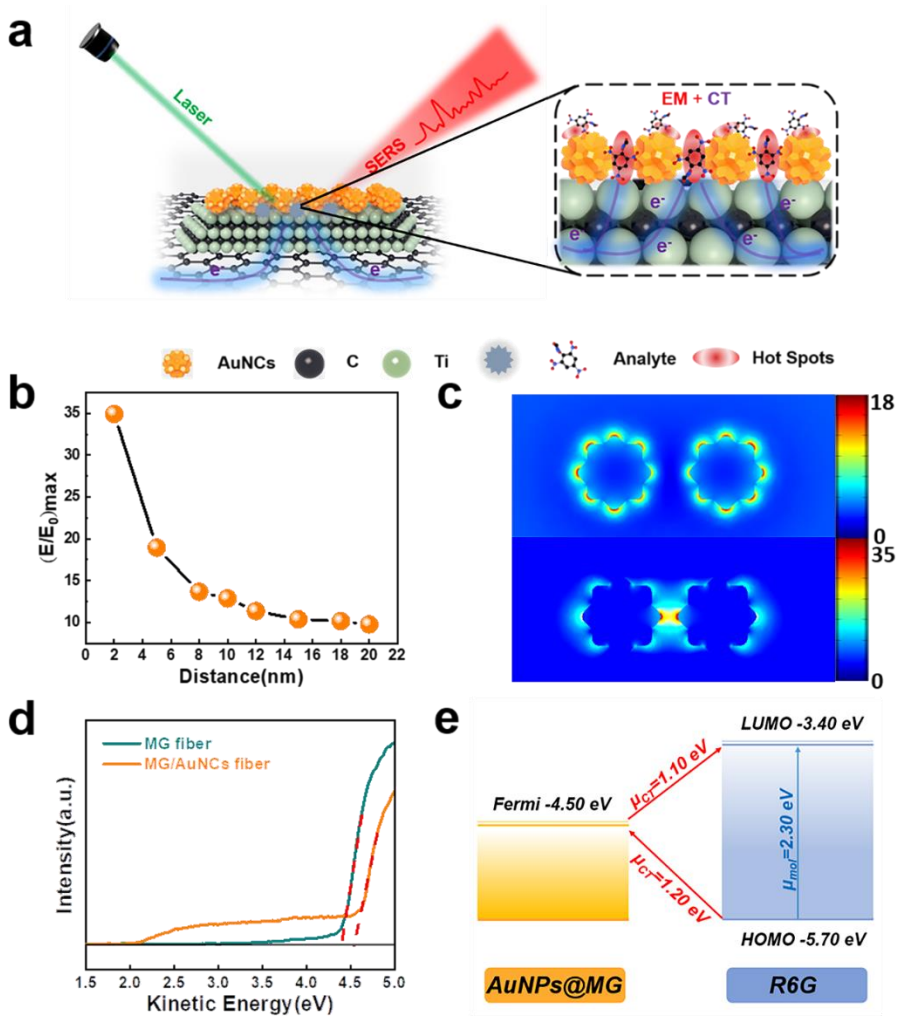

Figure 6. Proposed dual enhancement mechanisms of the MG/AuNCs-1 fiber substrate. (a) Schematic illustration of the SERS detection of the probing analytes on the MG/AuNCs surface. (b) Electric field distribution versus distance of adjacent AuNCs simulated by the FEM method. (c) Simulated electric field distribution of AuNCs on MG fibers and intensity as a function of the

distance of AuNCs. (d) UPS spectra for MG/AuNCs fiber. (e) Energy level diagram showing a charge-transfer process between R6G and the MG/AuNCs fiber substrate.

The intensity and spatial distribution of the electromagnetic field at the vicinity of the decreased gap were calculated as presented in **Figure 6b and c**. At a large gap size, the electromagnetic intensity and corresponding EF_{sim} calculated is 1.05×10^5, which mainly results from the corners of a single AuNC. However, as the gap size decreases, a strong electric field is triggered from the plasmonic coupling of adjacent AuNCs (**Figure 6c**), resulting in a maximum EF_{sim} of 1.50×10^6. Thus, in our case, the Raman intensity of R6G molecules on the MG/AuNCs fiber substrates demonstrates a similar trend as the theories' results, where the distribution of AuNCs on the MG fibers varied from a sparse state to a dense state.

For these MG/AuNCs fiber substrates, apart from the electromagnetic (EM) mechanism, the chemical mechanism (CM) related to the photo-induced charge transfer (PICT) between the substrate and target analytes also plays a crucial role. To verify the CT effect of the R6G and MG/AuNCs fiber substrates, the UV-Vis absorption spectra of pure R6G and $T_3C_2T_x$ MXene@R6G hybrid solutions are shown in **Figure S9a**. Compared to the pure R6G molecules, the position of the main absorption peak of MXene-absorbed R6G solution has a redshift from 526 to 543 nm, which supports that the photo-induced charge transfer (PICT) (CM effect) will occur from the MG/AuNCs fiber substrates to the probe molecules[48, 49]. Furthermore, the involvement of AuNCs was also discussed. Unfortunately, as shown in **Figure S9b**, although the peak position of R6G was still observed to be shifted, it was difficult to exclude the interference of

AuNCs due to the peak of R6G was too close with AuNCs. Moreover, the electronic properties of the SERS substrate were also characterized by ultraviolet photoelectron spectroscopy (UPS) (**Figure 6d**), and the work function (WF) of the MG and MG/AuNCs-1 fiber were deduced to be 4.4 and 4.5 eV respectively via UPS curves. Compared with MG fibers, the increased WF of MG/AuNCs-1 due to the introduction of Au (WF=5.1 ev). Thus, the Fermi level is further calculated by formula (2):

$$\varphi = E_V - E_F \tag{2}$$

where φ is WF, E_v is the vacuum level = 0 eV, and E_F is the Fermi level. According to the Herzberg-Teller rules[50, 51], the energy level diagram of the MG/AuNCs fiber and R6G systems is shown in **Figure 6e**. In general, two transitions are involved in this process, the intramolecular transition (μ_{mol} = 2.30 eV) from the highest occupied atomic orbital (HOMO) of R6G molecules to the lowest unoccupied molecular orbital (LUMO), and the CT transition will automatically occur from the HOMO of the R6G to MG/AuNCs (μ_{ct} = 1.10 eV) and vice versa (μ_{ct} =1.20 eV). They are all less than the energy of the 532 nm laser (~2.33 eV), which will generate a strong resonance-enhanced Raman signal under excitation. Notably, MG fiber has a large density of states near the Fermi level to provide a greater electron transition probability and faster charge transfer, contributing 4.71×10^3 to EF_{exp} (**Figure S10**). Based on the above results, the SERS mechanism of MG/AuNCs-1 fiber is described as the synergistic enhancement mechanism of EM (1.50×10^6) and CM (4.71×10^3), which is almost consistent with the experimental result at EF_{exp} of R6G molecules (2.01×10^9) onto the MG/AuNCs-1 fiber substrate (**Table S1**).

Nitroaromatic explosive such as 2, 4, 6-trinitrotoluene (TNT) is the most commonly used explosive in military and terrorist activities and cause environmental concern by contaminating soil and groundwater[52]. As evidenced by previous reports[53], L-cysteine modified Au nanoparticles can form Meisenheimer complex with TNT, which provides the possibility for the selective detection of such electron-deficient nitro-aromatic explosives. In our work, functionalization was accomplished by immersing MG/AuNCs-1 fiber in L-cysteine solution (noted as MG/AuNCs-1-C) for 24 h to achieve specificity for nitroaromatic explosives, as demonstrated in **Figure 7a**.

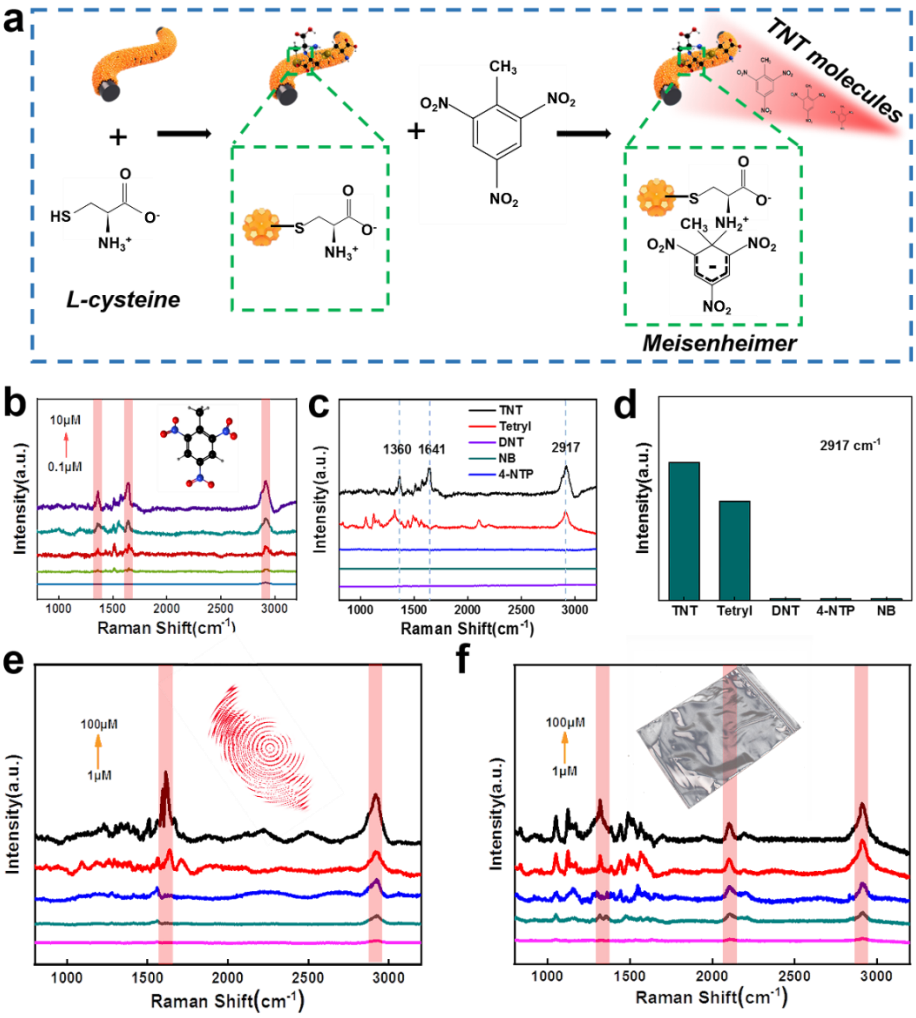

Figure 7. (a) Schematic representation of the modification of MG/AuNCs-1 fiber substrate by L-

cysteine and the corresponding selective detection of TNTs. (b) SERS spectra of TNT with different concentrations on the MG/AuNCs-1-C fiber substrate. (c) SERS spectra of different target molecules, such as TNT, tetryl, 2,4-dinitrotoluene (DNT), nitrobenzene (NB) and 4-nitrophenol (4-NTP), collected from the MG/AuNCs-1-C fiber substrate and (d) corresponding comparison of SERS intensity at the characteristic peak of 2917 cm^{-1}. SERS spectra of TNT (e) and Tetryl (f) with different concentrations (such as 1, 5, 10, 50 and 100 μM) on the MG/AuNCs-1-C fiber substrate collected from the fingerprint and sample bag. Inset in (a) and (b): photographs of the fingerprint and sample bag, respectively.

Figure S11 demonstrates the infrared spectrum of the vibrations of MG/AuNCs-1-C fibers. The S-H, C-S and C-N bonds near 570, 851, and 1243 cm^{-1} can be observed, indicating the successful modification of fibers by L-cysteine molecules. Moreover, to verify the performance of the as-synthesized flexible substrate, the SERS spectra of standard TNT acetonitrile solutions (from 0.1 μM to 10 μM) added to the MG/AuNCs-1-C fiber substrate were detected, as shown in **Figure 7b**. Spectra at all concentrations distinctively discerned the characteristic peaks, which correspond to NO_2 symmetric stretching vibration (1360 cm^{-1}), C=C aromatic stretching vibration (1638 cm^{-1}), and NH^{2+} stretching, CH stretching, and CH_2 asymmetric stretching vibration at broad peaks (approximately 2917 cm^{-1}) respectively, whereas all characteristic peaks cannot be observed in unmodified MG/AuNCs-1 fiber (**Figure S12**). This further verifies the successful modification of L-cysteine molecules on the fiber and trace detection for TNT molecules via the formation of the Meisenheimer complex. Meanwhile, the intensity of the 2917 cm^{-1} peak is highly correlated with the concentration of TNT (R^2

= 0.976) (**Figure S13)**, and its Raman signal can still be found at low concentration of 0.1 μM (**Figure S14**), revealing that the flexible MG/AuNCs-1-C fiber SERS substrate has excellent sensitivity and application potential in the quantitative detection of TNT explosives.

Distinguishing the target molecules from suspicious samples with complex components is very essential in practical applications. First, we evaluated the SERS performance of the MG/AuNCs-1-C fiber substrate for detecting the TNT derivative (tetryl, 2,4-dinitrotoluene) and potential interfering substances (4-NTP, NB, R6G), as demonstrated in **Figure 7c.** The characteristic peak at 2917 cm^{-1} from various nitroaromatic compounds, demonstrates that the flexible SERS substrate is selective for electron-deficient nitro explosives such as TNT and Tetryl, due to the formation of the Meisenheimer complex (**Figure 7d**). Moreover, the ability to detect TNT was investigated under the interference of R6G, which has a strong SERS signal at the fingerprint region (500~1800 cm^{-1}). As shown in **Figure S15**, the characteristic peaks at 1360 $cm^{-1}$and 1638 $cm^{-1}$are masked, but the existence of TNT can still be observed in the characteristic peak of 2917 cm^{-1}.

As a demonstration, TNT molecules on the fingerprint and sample bag were also be probed to show the potential application in flexible fiber SERS sensors. **Figure 7e and f** illustrate the SERS spectra of different concentrations of TNT (from 1 μM to 100 μM) collected from fingerprints and sample bags. Although the Raman peaks of other impurities interfere with the sample signal, TNT can still be detected by the characteristic peak of the Meisenheimer complex at 1360, 1638 and 2917 cm^{-1}. Our

results indicate that the MG/AuNCs-1-C fiber could specifically detect nitroaromatic explosives from samples. In fact, the detection limit is less than 1 μM due to the loss in operation, but still lower than that of widely used chromatography[54, 55]. Considering the analysis time and scope of application, the MG/AuNCs-1-C fiber is expected to realize fast and portable detection of TNT explosives.

Conclusion

In summary, we have demonstrated a facile and novel way to produce flexible and free-standing SERS MG/AuNCs fiber substrates, where the uniform and dense AuNCs were in-situ reduced on the surface of mechanical-stable MG fibers by adjusting the GO content and the amounts of Au^{3+} cations. The MG/AuNCs-1 fiber exhibited a low detection limit of 10^{-11} M with a high EF_{exp} of 2.01×10^{9}, a good Raman signal homogeneity (the average RSD values around at 9.56%) for the monitoring of R6G molecules. Furthermore, thanks to the anchoring of anti-oxidative AuNCs on the MG fibers and paramount bonding between them, the fiber SERS-active substrate remains 75% intensity at 612 cm^{-1} for 90 days of storage. Meanwhile, the fiber substrate demonstrated a stable Raman signal even under physical deformation stimuli for 500 cycles bending and twisting, due to the strong bonding between the MG fiber and AuNCs, and excellent mechanical stability of MG substrate material. Both experimental and simulations results quantified the synergistic contributions of EM and CT to EF_{exp}, which provides a new insight into the SERS enhancement mechanism of 2D materials and noble metal flexible composite. Additionally, for the actual

applications, ultralow concentrations of TNT (0.1 μM) in complex analytes can be selectively detected through L-cysteine-modified MG/AuNCs-1 fibers, even on fingerprints or sample bags. Thus, this easy and efficient fabrication technique for flexible fiber SERS substrate on a large scale can be used for the monitoring the probe molecules for wide applications in ultrasensitive environmental sensing and explosive recognition at national security.

Supporting Information

Supporting Information is available free of charge from the XXX.

• TEM and AFM images of GO and $Ti_3C_2T_x$ MXene nanosheets; Tension strength of MG fibers; SEM images of MG/AuNCs fibers; SERS spectrum of R6G molecules on the MG/AuNCs-1 fiber; Optical image and Raman mapping of the MG/AuNCs-1 fiber for R6G molecules; XRD patterns of MG fiber exposed to air for different time; SEM image of MG/AuNCs-1 fiber after 500 bending cycles; Comparison of UV-vis spectra of samples; SERS spectra of R6G on the pure MG fiber; Infrared spectrum of MG/AuNCs-1-C fiber; SERS spectra of TNT on MG/AuNCs-1 fiber before and after modification; The relationship between SERS intensity and TNT; SERS spectrum of R6G and TNT molecules on MG/AuNCs-1-C fiber; Characterization of $Ti_3C_2T_x$ MXene@AuNCs hybrids; The digital image of $Ti_3C_2T_x$ MXene colloidal suspensions; The SEM image of single AuNC on MG fiber; SEM images of MG/AuNCs fibers; Size distribution of AuNCs on the MG fibers; Coverage of AuNCs on MG fiber, and relationship between the size of AuNCs and their corresponding density as functions of different concentrations of $HAuCl_4$; SERS spectra of 10^{-4} M R6G on the MG/AuNCs fibers; Cross-sectional SEM images of MG/AuNCs-1 fiber and their corresponding EDS mapping of Ti and Au elements.

File name: Plasmonic Coupling of Au Nanoclusters on a Flexible MXene/Graphene Oxide Fiber for Ultra-sensitive SERS Sensing.

Author contributions:

X. L. and A. D. conceived the idea and designed the experiments. X.L. performed the experiments. Y. S, W. D., S. W., T. Z. and H. L. helped with the experiments. A. D. and

T. L. supervised the work. X. L., A.D., A. Z. and T. C. L. drafted the manuscript, and all the authors contributed to the editing of the manuscript.

Acknowledgments:

We acknowledge support by the Natural Science Foundation of China (52072302, 51802267, 51872235), the Science and Technology Plan Project from Xi'an (22GXFW0135), and the China Postdoctoral Science Foundation (2020M673475).

References

1. Langer, J.; Jimenez de Aberasturi, D.; Aizpurua, J.; Alvarez-Puebla, R. A.; Auguié, B.; Baumberg, J. J.; Bazan, G. C.; Bell, S. E. J.; Boisen, A.; Brolo, A. G.; Choo, J.; Cialla-May, D.; Deckert, V.; Fabris, L.; Faulds, K.; García de Abajo, F. J.; Goodacre, R.; Graham, D.; Haes, A. J.; Haynes, C. L.; Huck, C.; Itoh, T.; Käll, M.; Kneipp, J.; Kotov, N. A.; Kuang, H.; Le Ru, E. C.; Lee, H. K.; Li, J.-F.; Ling, X. Y.; Maier, S. A.; Mayerhöfer, T.; Moskovits, M.; Murakoshi, K.; Nam, J.-M.; Nie, S.; Ozaki, Y.; Pastoriza-Santos, I.; Perez-Juste, J.; Popp, J.; Pucci, A.; Reich, S.; Ren, B.; Schatz, G. C.; Shegai, T.; Schlücker, S.; Tay, L.-L.; Thomas, K. G.; Tian, Z.-Q.; Van Duyne, R. P.; Vo-Dinh, T.; Wang, Y.; Willets, K. A.; Xu, C.; Xu, H.; Xu, Y.; Yamamoto, Y. S.; Zhao, B.; Liz-Marzán, L. M., Present and Future of Surface-Enhanced Raman Scattering. *ACS Nano* **2020,** *14* (1), 28-117.

2. Chio, W.-I. K.; Xie, H.; Zhang, Y.; Lan, Y.; Lee, T.-C., SERS biosensors based on cucurbituril-mediated nanoaggregates for wastewater-based epidemiology. *TrAC Trends in Analytical Chemistry* **2022,** *146*, 116485.

3. Ding, S.-Y.; You, E.-M.; Tian, Z.-Q.; Moskovits, M., Electromagnetic theories of surface-enhanced Raman spectroscopy. *Chemical Society Reviews* **2017,** *46* (13), 4042-4076.

4. Jeong, H.-H.; Choi, E.; Ellis, E.; Lee, T.-C., Recent advances in gold nanoparticles for biomedical applications: from hybrid structures to multi-functionality. *Journal of Materials Chemistry B* **2019,** *7* (22), 3480-3496.

5. Dang, A.; Wang, Y.; Zhang, H.; Panatdasirisuk, W.; Xia, Y.; Wang, Z.; Jariwala, D.; Li, T.; Yang, S., Electrospun Gold Nanoprism/Poly(vinyl alcohol) Nanofibers for Flexible and Free-Standing Surface-Enhanced Raman Scattering Substrates. *ACS Applied Nano Materials* **2022,** *5* (5), 6650-6658.

6. Chio, W.-I. K.; Liu, J.; Jones, T.; Perumal, J.; Dinish, U. S.; Parkin, I. P.; Olivo, M.; Lee, T.-C., SERS multiplexing of methylxanthine drug isomers via host–guest size matching and machine learning. *Journal of Materials Chemistry C* **2021,** *9* (37), 12624-12632.

7. Taylor, R. W.; Lee, T.-C.; Scherman, O. A.; Esteban, R.; Aizpurua, J.; Huang, F. M.; Baumberg, J. J.; Mahajan, S., Precise Subnanometer Plasmonic Junctions for SERS within Gold Nanoparticle Assemblies Using Cucurbit[n]uril "Glue". *ACS Nano* **2011,** *5* (5), 3878-3887.

8. Zhao, Y.-Y.; Ren, X.-L.; Zheng, M.-L.; Jin, F.; Liu, J.; Dong, X.-Z.; Zhao, Z.-S.; Duan, X.-M., Plasmon-enhanced nanosoldering of silver nanoparticles for high-conductive nanowires

electrodes. *Opto-Electronic Advances* **2021,** *4* (12), 200101-1-200101-9.
9. Wang, X.; Shi, W.; Jin, Z.; Huang, W.; Lin, J.; Ma, G.; Li, S.; Guo, L., Remarkable SERS Activity Observed from Amorphous ZnO Nanocages. *Angewandte Chemie International Edition* **2017,** *56* (33), 9851-9855.
10. Ji, C.; Lu, J.; Shan, B.; Li, F.; Zhao, X.; Yu, J.; Xu, S.; Man, B.; Zhang, C.; Li, Z., The Origin of Mo2C Films for Surface-Enhanced Raman Scattering Analysis: Electromagnetic or Chemical Enhancement? *The Journal of Physical Chemistry Letters* **2022,** *13* (38), 8864-8871.
11. Zhang, C.; Li, Z.; Qiu, S.; Lu, W.; Shao, M.; Ji, C.; Wang, G.; Zhao, X.; Yu, J.; Li, Z., Highly ordered arrays of hat-shaped hierarchical nanostructures with different curvatures for sensitive SERS and plasmon-driven catalysis. *Nanophotonics* **2022,** *11* (1), 33-44.
12. Zhang, C.; Ji, C.; Yu, J.; Li, Z.; Li, Z.; Li, C.; Xu, S.; Li, W.; Man, B.; Zhao, X., MoS2-based multiple surface plasmonic coupling for enhanced surface-enhanced Raman scattering and photoelectrocatalytic performance utilizing the size effect. *Opt. Express* **2021,** *29* (23), 38768-38780.
13. Yu, T.-H.; Ho, C.-H.; Wu, C.-Y.; Chien, C.-H.; Lin, C.-H.; Lee, S., Metal–organic frameworks: a novel SERS substrate. *Journal of Raman Spectroscopy* **2013,** *44* (11), 1506-1511.
14. Xu, W.; Mao, N.; Zhang, J., Graphene: A Platform for Surface-Enhanced Raman Spectroscopy. *Small* **2013,** *9* (8), 1206-1224.
15. Cai, Q.; Mateti, S.; Yang, W.; Jones, R.; Watanabe, K.; Taniguchi, T.; Huang, S.; Chen, Y.; Li, L. H., Boron Nitride Nanosheets Improve Sensitivity and Reusability of Surface-Enhanced Raman Spectroscopy. *Angewandte Chemie International Edition* **2016,** *55* (29), 8405-8409.
16. Sarycheva, A.; Makaryan, T.; Maleski, K.; Satheeshkumar, E.; Melikyan, A.; Minassian, H.; Yoshimura, M.; Gogotsi, Y., Two-Dimensional Titanium Carbide (MXene) as Surface-Enhanced Raman Scattering Substrate. *The Journal of Physical Chemistry C* **2017,** *121* (36), 19983-19988.
17. Soundiraraju, B.; George, B. K., Two-Dimensional Titanium Nitride (Ti2N) MXene: Synthesis, Characterization, and Potential Application as Surface-Enhanced Raman Scattering Substrate. *ACS Nano* **2017,** *11* (9), 8892-8900.
18. He, Z.; Rong, T.; Li, Y.; Ma, J.; Li, Q.; Wu, F.; Wang, Y.; Wang, F., Two-Dimensional TiVC Solid-Solution MXene as Surface-Enhanced Raman Scattering Substrate. *ACS Nano* **2022,** *16* (3), 4072-4083.
19. Karthick Kannan, P.; Shankar, P.; Blackman, C.; Chung, C.-H., Recent Advances in 2D Inorganic Nanomaterials for SERS Sensing. *Advanced Materials* **2019,** *31* (34), 1803432.
20. Fleischmann, M.; Hendra, P. J.; McQuillan, A. J., Raman spectra of pyridine adsorbed at a silver electrode. *Chemical Physics Letters* **1974,** *26* (2), 163-166.
21. Fang, Y.; Seong, N.-H.; Dlott, D. D., Measurement of the Distribution of Site Enhancements in Surface-Enhanced Raman Scattering. *Science* **2008,** *321* (5887), 388-392.
22. Kim, J.; Song, X.; Ji, F.; Luo, B.; Ice, N. F.; Liu, Q.; Zhang, Q.; Chen, Q., Polymorphic Assembly from Beveled Gold Triangular Nanoprisms. *Nano Letters* **2017,** *17* (5), 3270-3275.
23. Ye, Z.; Li, C.; Chen, Q.; Xu, Y.; Bell, S. E. J., Self-assembly of colloidal nanoparticles into 2D arrays at water–oil interfaces: rational construction of stable SERS substrates with accessible enhancing surfaces and tailored plasmonic response. *Nanoscale* **2021,** *13* (12), 5937-5953.
24. He, D.; Hu, B.; Yao, Q.-F.; Wang, K.; Yu, S.-H., Large-Scale Synthesis of Flexible Free-Standing SERS Substrates with High Sensitivity: Electrospun PVA Nanofibers Embedded with Controlled

Alignment of Silver Nanoparticles. *ACS Nano* **2009,** *3* (12), 3993-4002.
25. Liu, X.; Ma, J.; Jiang, P.; Shen, J.; Wang, R.; Wang, Y.; Tu, G., Large-Scale Flexible Surface-Enhanced Raman Scattering (SERS) Sensors with High Stability and Signal Homogeneity. *ACS Applied Materials & Interfaces* **2020,** *12* (40), 45332-45341.
26. Xu, K.; Zhou, R.; Takei, K.; Hong, M., Toward Flexible Surface-Enhanced Raman Scattering (SERS) Sensors for Point-of-Care Diagnostics. *Advanced Science* **2019,** *6* (16), 1900925.
27. Li, Z.; Huang, X.; Lu, G., Recent developments of flexible and transparent SERS substrates. *Journal of Materials Chemistry C* **2020,** *8* (12), 3956-3969.
28. Chen, J.; Huang, Y.; Kannan, P.; Zhang, L.; Lin, Z.; Zhang, J.; Chen, T.; Guo, L., Flexible and Adhesive Surface Enhance Raman Scattering Active Tape for Rapid Detection of Pesticide Residues in Fruits and Vegetables. *Analytical Chemistry* **2016,** *88* (4), 2149-2155.
29. Qin, X.; Si, Y.; Wang, D.; Wu, Z.; Li, J.; Yin, Y., Nanoconjugates of Ag/Au/Carbon Nanotube for Alkyne-Meditated Ratiometric SERS Imaging of Hypoxia in Hepatic Ischemia. *Analytical Chemistry* **2019,** *91* (7), 4529-4536.
30. Lee, M.; Oh, K.; Choi, H.-K.; Lee, S. G.; Youn, H. J.; Lee, H. L.; Jeong, D. H., Subnanomolar Sensitivity of Filter Paper-Based SERS Sensor for Pesticide Detection by Hydrophobicity Change of Paper Surface. *ACS Sensors* **2018,** *3* (1), 151-159.
31. Alexander, K. D.; Skinner, K.; Zhang, S.; Wei, H.; Lopez, R., Tunable SERS in Gold Nanorod Dimers through Strain Control on an Elastomeric Substrate. *Nano Letters* **2010,** *10* (11), 4488-4493.
32. Fortuni, B.; Inose, T.; Uezono, S.; Toyouchi, S.; Umemoto, K.; Sekine, S.; Fujita, Y.; Ricci, M.; Lu, G.; Masuhara, A.; Hutchison, J. A.; Latterini, L.; Uji-i, H., In situ synthesis of Au-shelled Ag nanoparticles on PDMS for flexible, long-life, and broad spectrum-sensitive SERS substrates. *Chemical Communications* **2017,** *53* (82), 11298-11301.
33. VahidMohammadi, A.; Rosen, J.; Gogotsi, Y., The world of two-dimensional carbides and nitrides (MXenes). *Science* **2021,** *372* (6547), eabf1581.
34. Dang, A.; Sun, Y.; Liu, Y.; Xia, Y.; Liu, X.; Gao, Y.; Wu, S.; Li, T.; Zada, A.; Ye, F., Flexible Ti3C2Tx/Carbon Nanotubes/CuS Film Electrodes Based on a Dual-Structural Design for High-Performance All-Solid-State Supercapacitors. *ACS Applied Energy Materials* **2022,** *5* (7), 9158-9172.
35. Yin, L.; Li, Y.; Yao, X.; Wang, Y.; Jia, L.; Liu, Q.; Li, J.; Li, Y.; He, D., MXenes for Solar Cells. *Nano-Micro Letters* **2021,** *13* (1), 78.
36. Xie, H.; Li, P.; Shao, J.; Huang, H.; Chen, Y.; Jiang, Z.; Chu, P. K.; Yu, X.-F., Electrostatic Self-Assembly of Ti3C2Tx MXene and Gold Nanorods as an Efficient Surface-Enhanced Raman Scattering Platform for Reliable and High-Sensitivity Determination of Organic Pollutants. *ACS Sensors* **2019,** *4* (9), 2303-2310.
37. Satheeshkumar, E.; Makaryan, T.; Melikyan, A.; Minassian, H.; Gogotsi, Y.; Yoshimura, M., One-step Solution Processing of Ag, Au and Pd@MXene Hybrids for SERS. *Scientific Reports* **2016,** *6* (1), 32049.
38. Cheng, R.; Hu, T.; Hu, M.; Li, C.; Liang, Y.; Wang, Z.; Zhang, H.; Li, M.; Wang, H.; Lu, H.; Fu, Y.; Zhang, H.; Yang, Q.-H.; Wang, X., MXenes induce epitaxial growth of size-controlled noble nanometals: A case study for surface enhanced Raman scattering (SERS). *Journal of Materials Science & Technology* **2020,** *40*, 119-127.

39. Wang, C.; Cheng, R.; Hou, P.-X.; Ma, Y.; Majeed, A.; Wang, X.; Liu, C., MXene-Carbon Nanotube Hybrid Membrane for Robust Recovery of Au from Trace-Level Solution. *ACS Applied Materials & Interfaces* **2020,** *12* (38), 43032-43041.

40. Song, M.; Lyu, Y.; Guo, F.; Pang, S.-Y.; Wong, M.-C.; Hao, J., One-Step, DNA-Programmed, and Flash Synthesis of Anisotropic Noble Metal Nanostructures on MXene. *ACS Applied Materials & Interfaces* **2021,** *13* (44), 52978-52986.

41. Lim, K. R. G.; Shekhirev, M.; Wyatt, B. C.; Anasori, B.; Gogotsi, Y.; Seh, Z. W., Fundamentals of MXene synthesis. *Nature Synthesis* **2022,** *1* (8), 601-614.

42. Padmajan Sasikala, S.; Lim, J.; Kim, I. H.; Jung, H. J.; Yun, T.; Han, T. H.; Kim, S. O., Graphene oxide liquid crystals: a frontier 2D soft material for graphene-based functional materials. *Chemical Society Reviews* **2018,** *47* (16), 6013-6045.

43. Zhang, J.; Uzun, S.; Seyedin, S.; Lynch, P. A.; Akuzum, B.; Wang, Z.; Qin, S.; Alhabeb, M.; Shuck, C. E.; Lei, W.; Kumbur, E. C.; Yang, W.; Wang, X.; Dion, G.; Razal, J. M.; Gogotsi, Y., Additive-Free MXene Liquid Crystals and Fibers. *ACS Central Science* **2020,** *6* (2), 254-265.

44. Fang, B.; Chang, D.; Xu, Z.; Gao, C., A Review on Graphene Fibers: Expectations, Advances, and Prospects. *Advanced Materials* **2020,** *32* (5), 1902664.

45. Liu, R.; Jiang, L.; Yu, Z.; Jing, X.; Liang, X.; Wang, D.; Yang, B.; Lu, C.; Zhou, W.; Jin, S., MXene (Ti3C2Tx)-Ag nanocomplex as efficient and quantitative SERS biosensor platform by in-situ PDDA electrostatic self-assembly synthesis strategy. *Sensors and Actuators B: Chemical* **2021,** *333*, 129581.

46. Peng, Y.; Lin, C.; Long, L.; Masaki, T.; Tang, M.; Yang, L.; Liu, J.; Huang, Z.; Li, Z.; Luo, X.; Lombardi, J. R.; Yang, Y., Charge-Transfer Resonance and Electromagnetic Enhancement Synergistically Enabling MXenes with Excellent SERS Sensitivity for SARS-CoV-2 S Protein Detection. *Nano-Micro Letters* **2021,** *13* (1), 52.

47. Liu, L.; Shangguan, C.; Guo, J.; Ma, K.; Jiao, S.; Yao, Y.; Wang, J., Ultrasensitive SERS Detection of Cancer-Related miRNA-182 by MXene/MoS2@AuNPs with Controllable Morphology and Optimized Self-Internal Standards. *Advanced Optical Materials* **2020,** *8* (23), 2001214.

48. Li, J.; Yi, W.; Yin, M.; Yang, H.; Li, J.; Li, Y.; Jiao, Z.; Bai, H.; Zou, M.; Xi, G., Plasmonic Rare-Earth Nanosheets as Surface Enhanced Raman Scattering Substrates with High Sensitivity and Stability for Multicomponent Analysis. *ACS Nano* **2022,** *16* (1), 1160-1169.

49. Ge, Y.; Wang, F.; Yang, Y.; Xu, Y.; Ye, Y.; Cai, Y.; Zhang, Q.; Cai, S.; Jiang, D.; Liu, X.; Liedberg, B.; Mao, J.; Wang, Y., Atomically Thin TaSe2 Film as a High-Performance Substrate for Surface-Enhanced Raman Scattering. *Small* **2022,** *18* (15), 2107027.

50. Lombardi, J. R.; Birke, R. L., A Unified View of Surface-Enhanced Raman Scattering. *Accounts of Chemical Research* **2009,** *42* (6), 734-742.

51. Limbu, T. B.; Chitara, B.; Garcia Cervantes, M. Y.; Zhou, Y.; Huang, S.; Tang, Y.; Yan, F., Unravelling the Thickness Dependence and Mechanism of Surface-Enhanced Raman Scattering on Ti3C2TX MXene Nanosheets. *The Journal of Physical Chemistry C* **2020,** *124* (32), 17772-17782.

52. To, K. C.; Ben-Jaber, S.; Parkin, I. P., Recent Developments in the Field of Explosive Trace Detection. *ACS Nano* **2020,** *14* (9), 10804-10833.

53. Dasary, S. S. R.; Singh, A. K.; Senapati, D.; Yu, H.; Ray, P. C., Gold Nanoparticle Based Label-Free SERS Probe for Ultrasensitive and Selective Detection of Trinitrotoluene. *Journal of the American Chemical Society* **2009,** *131* (38), 13806-13812.

54. Salles, M. O.; Meloni, G. N.; de Araujo, W. R.; Paixão, T. R. L. C., Explosive colorimetric discrimination using a smartphone, paper device and chemometrical approach. *Analytical Methods* **2014,** *6* (7), 2047-2052.

55. Askim, J. R.; Li, Z.; LaGasse, M. K.; Rankin, J. M.; Suslick, K. S., An optoelectronic nose for identification of explosives. *Chemical Science* **2016,** *7* (1), 199-206.

Table of Contents

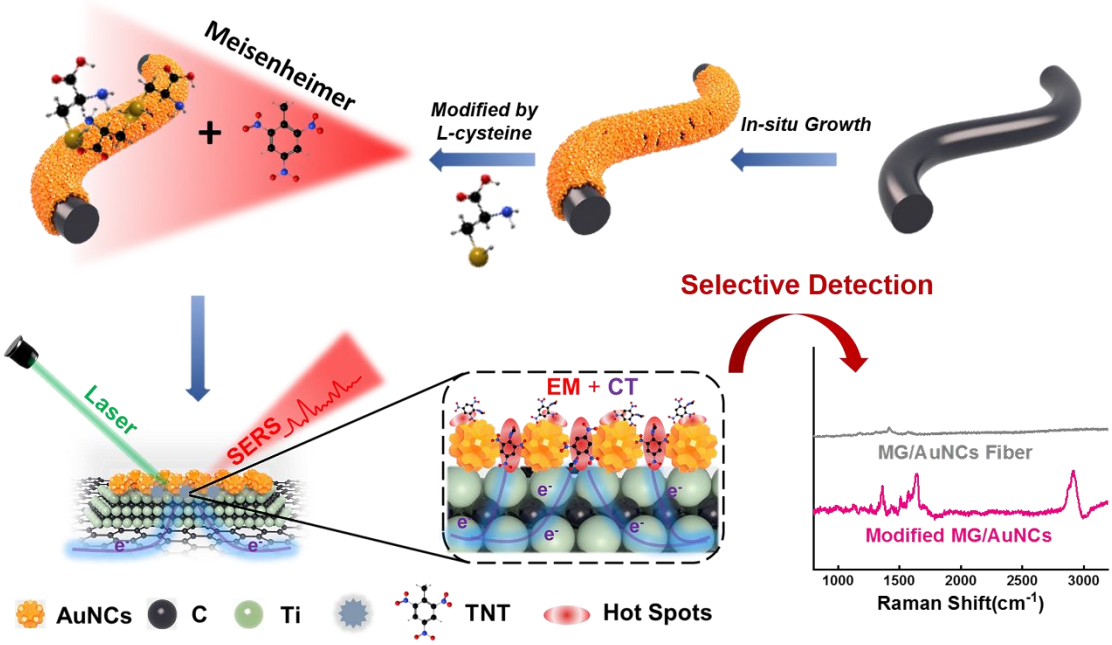

Plasmonic coupling of flexible MG/AuNCs fiber SERS substrate for selective sensing of explosive residues